

# Signatures of the spin Hall effect in hot and dense QCD matter

Baochi Fu,<sup>1,2,3,\*</sup> Long-Gang Pang,<sup>4,†</sup> Huichao Song,<sup>2,3,1,‡</sup> and Yi Yin<sup>5,6,§</sup>

<sup>1</sup>Center for High Energy Physics, Peking University, Beijing 100871, China

<sup>2</sup>Department of Physics and State Key Laboratory of Nuclear Physics and Technology, Peking University, Beijing 100871, China

<sup>3</sup>Collaborative Innovation Center of Quantum Matter, Beijing 100871, China

<sup>4</sup>Key Laboratory of Quark and Lepton Physics (MOE) and Institute of Particle Physics, Central China Normal University, Wuhan 430079, China

<sup>5</sup>Quark Matter Research Center, Institute of Modern Physics, Chinese Academy of Sciences, Lanzhou 730000, China

<sup>6</sup>University of Chinese Academy of Sciences, Beijing 100049, China

(Dated: February 1, 2022)

The spin Hall effect (SHE) is a generation of spin polarization for moving spin carriers in materials under an external electric field and has been observed in semiconductors, metals, and insulators at or below room temperature. Recent theoretical analyses show that spin Hall current can be induced by the baryon chemical potential gradient which plays the role of the analogous electric field and which becomes sizable in the fireballs created in heavy-ion collisions at beam energy of  $\mathcal{O}(10)$  GeV. In this letter, we study this important mechanism for spin polarization generation that has not been systematically explored before and predict the signature of the SHE in those collisions using a (3+1) D viscous hydrodynamic model MUSIC with AMPT initial condition. We propose to use the second Fourier coefficients of the net spin polarization of Lambda hyperon as sensitive probes to search for the SHE. Those SHE observables show a qualitative difference in both the sign and beam energy dependence for the situations with and without the SHE. Future experimental observation of these distinct qualitative features would provide strong evidence for the existence of the SHE in the hot and dense QCD matter at trillions of degrees.

**Introduction**— The spin Hall effect (SHE) is a quantum phenomenon that showcases the intriguing interplay between charge and spin degrees of freedom and probes transport properties in quantum materials [1, 2]. For a class of materials under an external electric field, the spin polarization of moving charge carriers can be generated by the SHE due to the Berry curvature of the charge carrier and relativistic spin-orbital coupling [3]. Since its first detection in 2004 [4], the SHE has been observed in semiconductors [4, 5], metals [6] and insulators [7]; see Ref. [2] for a review.

The materials mentioned above are at or below room temperature and are microscopically described by QED. In contrast, in this letter, we will study and predict the signatures of the SHE in the spin polarization of  $\Lambda$  hyperon (and  $\bar{\Lambda}$  anti-hyperon) produced in the extremely hot and dense QCD matter created in relativistic heavy-ion collisions where the spin carriers (quarks, gluons and/or hadrons) interact with each other through strong interaction in media at temperature above  $10^{12}$  K. Recently, the observation of  $\Lambda$  ( $\bar{\Lambda}$ ) polarization at Relativistic Heavy-ion Collider (RHIC) and Large Hadron Collider (LHC) [8–13] has inspired many studies on spin dynamics of QCD many-body physics, (see Refs. [9, 14] for reviews). While the “global” (phase space averaged) spin polarization is well-described by the effects of vorticity for a wide range of beam energy, the differential polarization measurements of the azimuthal angle dependence at top RHIC and LHC energies [12, 13] show sign opposite to the theory calculations based on thermal vorticity effects [15], see also Refs. [16–22] for examples of

studies on differential spin polarization at BES energies. Newly-discovered shear-induced polarization (SIP) [23–25] is found to be crucial for solving this “polarization sign puzzle” [24, 26]. Despite of those developments, the possible signature of the SHE has not been fully explored until now (see Refs. [27, 28] for previous investigation of the SHE).

Specifically, we shall consider the SHE induced by baryon chemical potential gradient  $\nabla\mu_B$  which becomes sizable in the fireballs created at colliding energy of  $\mathcal{O}(10)$  GeV. This phenomena as well as spin polarized by electric field has been predicted and quantitatively described within the framework of relativistic quantum kinetic equations [23, 29–33] and linear response theory [23, 27]. Just as charge current will be induced by both chemical potential gradient and electric field, the spin Hall current can be generated by  $\nabla\mu_B$  which plays an analogous role of the electric field [34]. That is, for a spin carrier of momentum  $\mathbf{p}$  with baryon charge  $q_B$ , the induced spin polarization vector  $\mathbf{P}$  is given by

$$\mathbf{P} \propto -\mathbf{p} \times (q_B \nabla\mu_B). \quad (1)$$

Eq. (1) shows that spin polarized by the SHE depends on momentum. Therefore one should look for the SHE signature in phase space distribution of polarization observables, i.e. the “local” spin polarization, rather than in the global polarization. In fact, the recent model calculations confirm the SHE contribution to the global spin polarization is small in magnitude [28].

In this letter, we present the first quantitative prediction of the SHE signals in differential spin polarization

that can be tested experimentally at RHIC beam energy scan (BES) energies. Using the freeze-out profiles generated from MUSIC viscous hydrodynamics with AMPT initial conditions, we calculate the spin polarization of  $\Lambda$  and  $\bar{\Lambda}$  hyperons along the beam direction  $\hat{z}$  and the out-plane direction  $\hat{y}$  in Au+Au collisions with the beam energy in the range  $\sqrt{s_{NN}} = 7.7$ -200 GeV. We find that the SHE gives rise to significant separation for the differential polarization between  $\Lambda$  and  $\bar{\Lambda}$ . The second harmonics of

$$\mathcal{A}^\mu(x, p) = \beta f_0(x, p)(1 - f_0(x, p))\varepsilon^{\mu\nu\alpha\rho} \times \left( \underbrace{\frac{1}{2}p_\nu \partial_\alpha^\perp u_\rho}_{\text{vorticity}} - \underbrace{\frac{1}{T}u_\nu p_\alpha \partial_\rho T}_{\text{T-gradient}} - \underbrace{\frac{p_\perp^2}{\varepsilon_0}u_\nu Q_\alpha^\lambda \sigma_{\rho\lambda}}_{\text{SIP}} - \underbrace{\frac{q_B}{\varepsilon_0\beta}u_\nu p_\alpha \partial_\rho(\beta\mu_B)}_{\text{SHE}} \right), \quad (2)$$

where  $f_0(x, p) = (e^{(\varepsilon_0 - q_B \mu_B)\beta} + 1)^{-1}$  is the Fermi-Dirac distribution function with  $\varepsilon_0 = p \cdot u$  and  $\beta = 1/T$ . Note  $q_B = 1$  for baryons and  $q_B = -1$  for anti-baryons. Here, we define  $\partial_\perp^\mu \equiv \Delta^{\mu\nu} \partial_\nu$ ,  $p_\perp^\mu \equiv \Delta^{\mu\nu} p_\nu$  with  $\Delta^{\mu\nu} = g^{\mu\nu} - u^\mu u^\nu$ . We denote momentum quadrupole by  $Q^{\mu\nu} = -p_\perp^\mu p_\perp^\nu / p_\perp^2 + \Delta^{\mu\nu}/3$  and shear stress tensor by  $\sigma^{\mu\nu} = \partial_\perp^{(\mu} u^{\nu)} - (1/3)\Delta^{\mu\nu}(\partial \cdot u)$ .

Eq. (2) includes all possible first order hydrodynamic gradient contributions to the spin polarization in phase space that are allowed by symmetry, except for the vorticity-quadrupole coupling which is found to be suppressed in perturbative calculations [23]. Among those four independent contributions, the first and second terms in the brackets represent the vorticity-induced and T-gradient induced polarization respectively. The combination of the two is proportional to the thermal vorticity, the effect of which has been widely studied previously [15, 35]. The recently-discovered shear-induced polarization (SIP) [23–25, 33] is shown in the third term. The SHE contribution, given by the last term, is of potential importance for baryon-rich QCD matter. We shall employ Eq. (2) as a basis for the subsequently systematic analysis of spin polarization at BES energies.

To compute the spin polarization of the produced  $\Lambda$  and  $\bar{\Lambda}$  hyperons on the freezeout-surface  $\Sigma_\mu$  from the axial Wigner function, we follow the widely-used prescription [35, 36]:

$$P^\mu(\mathbf{p}) = \frac{\int d\Sigma^\alpha p_\alpha \mathcal{A}^\mu(x, \mathbf{p}; m)}{2m \int d\Sigma^\alpha p_\alpha f_0(x, p)}, \quad (3)$$

where the factor 2 in the denominator comes from the degeneracy of spin 1/2 fermions.

The hydrodynamic profile on the freeze-out surface is generated by 3+1 dimensional viscous hydrodynamics MUSIC. The initial energy-momentum tensor  $T^{\mu\nu}(x)$  and net baryon number density  $n_B(x)$  are obtained from AMPT model [37, 38] with Gaussian smearing at proper time  $\tau_0$  [39] after average over more than  $10^5$  events

the net spin polarization can be utilized as unambiguous observables to search for the SHE.

**Method**— In field theory, the phase space density of spin polarization of a fermion/anti-fermion with mass  $m$  and four-momentum  $p^\mu$  is described by the corresponding axial Wigner function  $\mathcal{A}^\mu(x, p)$ . To the first order in the gradient of hydrodynamic variables, i.e., temperature  $T$ , flow velocity  $u^\mu$ , chemical potential  $\mu_B$ ,  $\mathcal{A}^\mu$  for a baryon-rich fluid is given by [23, 27] (see also Refs. [31, 33]):

$\sqrt{s_{NN}}$ [GeV]	$c_N$	$\eta/s$	$\tau_0$ [fm/c]	$\varepsilon_{SW}$ [GeV/fm <sup>3</sup> ]
7.7	1.8	0.16	2.0	0.35
19.6	1.8	0.12	1.2	0.45
27	1.8	0.10	1.0	0.50
62.4	1.9	0.08	0.6	0.60
200	1.9	0.08	0.4	0.65

TABLE I. The subset of parameters used in hydrodynamic simulations, see text.

at each  $\sqrt{s_{NN}}$ . We have multiplied  $T^{\mu\nu}$  obtained from AMPT by a phenomenological normalization factor  $c_N$  which is tuned to match with charged hadron production in most central collisions. The hydrodynamic evolution ends when energy density reaches a fixed value  $\varepsilon_{SW}$ . Table I lists relevant parameters used in our calculation of hydrodynamic profiles. Unless noted in Table. I, the model set-up for AMPT+MUSIC are the same as our previous studies [20, 24].

Given significant uncertainties in the current understanding of the hadronization of spin polarization and its subsequent hadronic evolution, we consider two benchmark scenarios: the ‘‘Lambda equilibrium’’ and ‘‘strange memory’’ [24]. The former assumes that the spin of  $\Lambda$  immediately responds to the hydrodynamic gradients [16, 20, 40]. In contrast, the latter supposes that the spin of  $\Lambda$  inherits that of the strange quark and is frozen after the hadronization [41–43]. In practice, we input  $m = 1.116$  GeV,  $q_B = \pm 1$  and  $m = 0.3$  GeV,  $q_B = 1/3$  in Eq. (3) for the ‘‘Lambda equilibrium’’ and ‘‘strange memory’’ scenario respectively, as we did in Ref. [24]. Clearly, those two scenarios represent two extremes, i.e., the spin relaxation time of  $\Lambda$  is very short  $\tau_{\text{spin}} \rightarrow 0$  and very long  $\tau_{\text{spin}} \rightarrow \infty$ , respectively, with the reality (possibly) sitting somewhere in between. However, as we shall see below, the main feature of the SHE observables that we propose is robust in both scenarios.

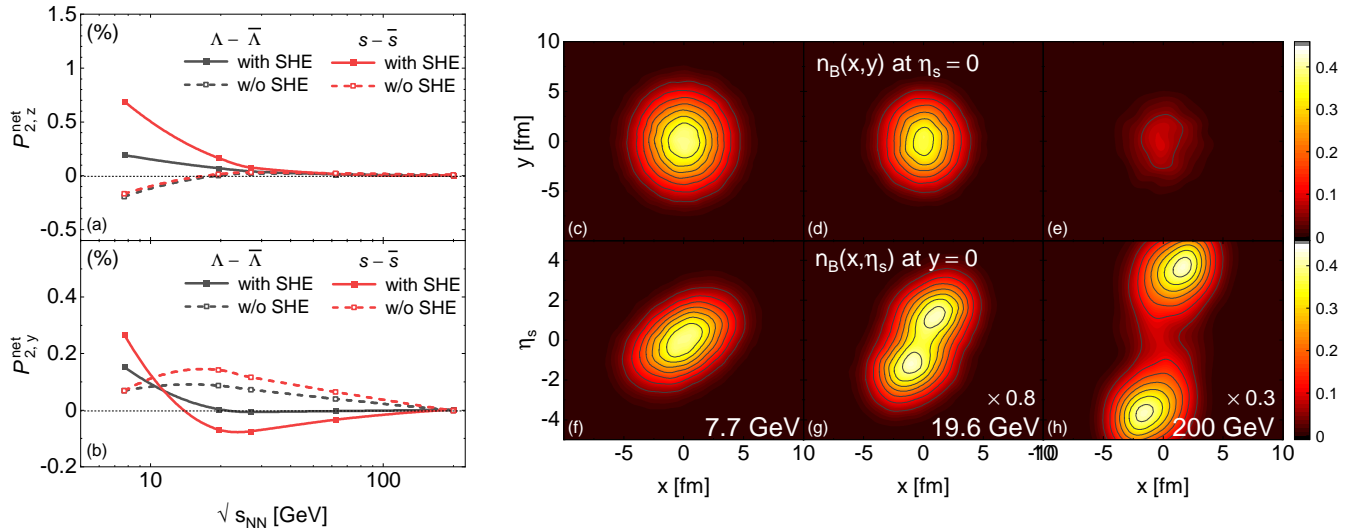


FIG. 1. Left panels: the collision energy dependence of second Fourier coefficients,  $P_{2,z}^{\text{net}}$  and  $P_{2,y}^{\text{net}}$ , for differential polarization of net  $\Lambda$  hyperons along the beam and out of plane direction, calculated in the “Lambda equilibrium” and “strange memory” scenarios, see text. Right panels: the initial net baryon density  $n_B$  on the transverse plane  $x - y$  at spatial rapidity  $\eta_s = 0$  and on the reaction plane  $x - \eta_s$  at  $y = 0$  in 20-50% Au+Au collisions at  $\sqrt{s_{NN}} = 7.7, 19.6, 200$  GeV.

**Results**— To devise the SHE observables, we shall rely on two observations followed from Eq. (2). First, as evident in this equation, the SHE distinguishes itself from the other contributions there since its sign depends on the baryon charge of the spin carrier. It is then natural to consider net  $\Lambda$  differential spin polarization  $P_{z,y}^{\text{net}}(\phi) \equiv P_{z,y}(\phi) - \bar{P}_{z,y}(\phi)$  to isolate the SHE contribution. Here  $P_{z,y}(\phi)$  and  $\bar{P}_{z,y}(\phi)$  is the polarization of  $\Lambda$  and  $\bar{\Lambda}$  hyperons as a function of azimuthal angle  $\phi$  along the out-of-plane direction ( $y$ ) and the beam direction ( $z$ ). Second, we notice that the SHE contribution is of a similar form to that of the T-gradient contribution with  $\partial_\mu T$  replaced by  $(q_B T^2 / \varepsilon_0) \partial_\mu (\beta \mu_B)$ . It has been demonstrated in a number of studies [15, 20, 24] that the effect of T-gradient will lead to a characteristic “ $\sin(2\phi)$ ” and “ $\cos(2\phi)$ ” pattern to  $P_z(\phi)$  and  $P_y(\phi)$  respectively. So we expect that the SHE would give rise to a similar sine/cosine pattern in differential polarization, with the sign depending on the typical direction of  $\mu_B$  gradient on the freezeout surface. Combining those observations, we designate the second harmonic component of  $P_{z,y}^{\text{net}}(\phi)$  in the Fourier decomposition to characterize the SHE signal:

$$P_{2,z}^{\text{net}} \equiv \langle P_z^{\text{net}}(\phi) \sin 2\phi \rangle, P_{2,y}^{\text{net}} \equiv -\langle P_y^{\text{net}}(\phi) \cos 2\phi \rangle \quad (4)$$

where  $\langle \dots \rangle$  denotes the average over the  $\phi$  angle.

The main results of this letter are shown in Fig. 1 (left) where the proposed SHE observables  $P_{2,z}^{\text{net}}$  and  $P_{2,y}^{\text{net}}$  as a function of collision energy are plotted for both “Lambda equilibrium” and “strange memory” scenarios. While the magnitude of those observables quantitatively depends

on the mass of spin carriers, we observe several distinctive traits which are robust in both scenarios. Without the SHE, the second sine harmonics of longitudinal net spin polarization  $P_{2,z}^{\text{net}}$  is negative at the beam energy of  $\mathcal{O}(10)$  GeV. With the SHE, it becomes positive and grows as collision energy decreases. Turning to the SHE observable in  $y$ -direction, we see a different non-monotonic collision energy dependence in situations with and without the SHE. As beam energy goes down,  $P_{2,y}^{\text{net}}$  shows an interesting sign change, from negative to positive, in the presence of the SHE. In contrast, this cosine coefficient would first increase to some positive value and then drop down when the SHE is absent. In short, we find that the proposed SHE observables show a marked difference in both sign and beam energy dependence with and without the SHE. Those striking qualitative features make us believe the predicted signatures provide crucial guidance for the future search for the SHE.

Physically, the SHE converts the spatial baryon chemical potential distribution into spin polarization in momentum space. Therefore, the characteristics of the baryon density profiles and their beam energy dependence would appear in observables sensitive to the SHE. To illustrate this, in Fig. 1 (right), we present initial baryon density distribution, which evolves hydrodynamically and can be converted to  $\mu_B$  through EoS. As Eq. (1) tells us, the spin vector polarized by the SHE is transverse to the gradient of  $\mu_B$ . So, to appreciate the behavior of  $P_{2,z}^{\text{net}}$ , we need to look at the  $n_B$  distribution in the  $x - y$  plane. We notice that the magnitude of  $n_B$  becomes larger with decreasing beam energy. Ac-

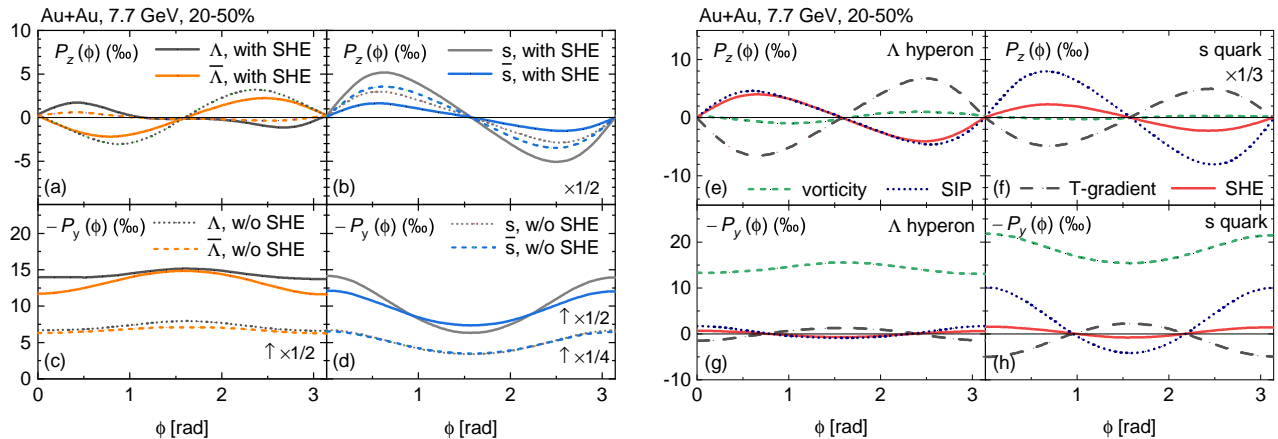


FIG. 2. Differential spin polarization  $P_z(\phi)$  and  $-P_y(\phi)$  calculated in the “Lambda equilibrium” (labeled by  $\Lambda, \bar{\Lambda}$ ) and the “strange memory” (labeled by  $s, \bar{s}$ ) scenarios in 20-50% Au+Au collision at  $\sqrt{s_{NN}} = 7.7$  GeV. Left panels: with and without the SHE contribution for  $\Lambda$  and  $\bar{\Lambda}$  hyperons. Right panels: The individual contribution from the vorticity, the T-gradient, the shear-induced polarization (SIP) and the SHE terms in Eq. (2) to the polarization of  $\Lambda$ .

cordingly, we see the growing trends of  $P_{2,z}^{\text{net}}$  when beam energy becomes smaller. Turning to the initial profile of  $n_B$  in the reaction plane  $x - \eta_s$  at  $y = 0$ , it transits from a double peak structure to a single peak structure from  $\sqrt{s_{NN}} = 200$  GeV to 7.7 GeV. This transition is anticipated from examining baryon stopping process at different collision energies [37, 44–47]. Such a qualitative change in baryon density profile will flip the sign of baryon density gradient along the longitudinal direction and is expected to induce the non-monotonic behaviors of  $P_{2,y}^{\text{net}}$ , as was confirmed quantitatively in Fig. 1 (left) [48].

It is worth emphasizing that even without the SHE,  $P_{2,z}^{\text{net}}, P_{2,y}^{\text{net}}$  is generically non-zero at BES energies. This is because there are other mechanisms for the spin polarization, such as the SIP, with magnitude depending on  $\mu_B$  through distribution function and Pauli blocking factor  $(1 - f)$  in Eq. (2). An important factor within the present model is that  $\Lambda$  tends to freeze-out later than  $\bar{\Lambda}$ , meaning  $\Lambda$  and  $\bar{\Lambda}$  probe the regimes with different hydrodynamic profiles. The resulting non-trivial non-SHE contribution necessitates a quantitative description of differential spin polarization by systematically including both the SHE and non-SHE effects, as was done for the first time in the present letter.

To complement Fig. 1, we show  $P_z(\phi), P_y(\phi)$  and  $\bar{P}_z(\phi), \bar{P}_y(\phi)$  at one representative beam energy  $\sqrt{s_{NN}} = 7.7$  GeV for both “ $\Lambda$  equilibrium” and “strange memory” scenarios in Fig. 2 (left). This figure exemplifies several characteristic features which are also present at other beam energies, see our coming publication for details [49]. First, azimuthal angle dependence of  $P_{z,y}(\phi)$  ( $\bar{P}_{z,y}(\phi)$ ) is mainly characterized by  $\cos(2\phi), \sin(2\phi)$  pattern. This supports choosing the second harmonics of

differential polarization to detect the SHE. Second, the SHE leads to a sizable separation of  $\Lambda$  and  $\bar{\Lambda}$  differential polarization. Without the SHE, either the difference between them is small, or the ordering is opposite to that with the SHE. For example, in “ $\Lambda$  equilibrium” scenario, the splitting between  $P_y(\phi)$  and  $\bar{P}_y(\phi)$ , shown in the bottom-left panel of Fig. 2 (left), is small in the absence of the SHE but becomes much larger once the SHE contribution is included. Meanwhile, the hierarchy between  $P_z(\phi), \bar{P}_z(\phi)$  will be reversed with and without the SHE. Similar qualitative features can equally be seen in the “strange memory” scenario, per the lessons we have just discussed when presenting Fig. 1.

In Fig. 2 (right), we present each of the four contributions, i.e., from the SIP, the T-gradient and the vorticity in addition to the SHE, to  $P_{y,z}$  at  $\sqrt{s_{NN}} = 7.7$  GeV. For longitudinal polarization  $P_z(\phi)$ , the vorticity contribution is insignificant. Similar to results of hydrodynamic calculations at top RHIC and LHC energies [24, 26], the sign of the second sine harmonics of the SIP and the T-gradient contribution is opposite to each other at the lower beam energies. The sign of the SHE contribution, as shown in red curve, is positive and is the same as that from the SIP. Overall, the sign of second sine harmonics of  $P_z$  will be determined by the competition among the SHE, the SIP and the T-gradient induced polarization. Turning to the polarization along  $y$ -direction, the “global” polarization is non-zero mainly because of the vorticity effect. Once again, the sign of the second cosine harmonics is driven by the competition among contributions from different hydrodynamic gradients. We note that while the sign of the SIP, T-gradient and vorticity contribution at  $\sqrt{s_{NN}} = 7.7$  GeV is same as that at top RHIC and LHC [24, 26], the sign of the

SHE contribution to  $P_y(\phi)$  is sensitive to the  $\mu_B$  profile in the longitudinal direction and hence can change from negative to positive with decreasing beam energy, as we discussed earlier. The main insight provided by Fig. 2 (right) is that the SHE contribution is indispensable for studying differential spin polarization at lower beam energies. The net spin polarization is more sensitive to the unique feature of the SHE than  $P_{z,y}$  or  $\bar{P}_{z,y}$  because the former largely isolates the effects of chemical potential gradient from other mechanisms for polarization generation.

Besides results presented above, we have investigated the consequences of changing the inputs in our hydrodynamic models. They include the initial baryon density and flow profile, shear viscosity, bulk viscosity, baryon diffusion constant, EoS, and freeze-out condition. We find that the SHE signal is mostly sensitive to the initial profile but those variations within realistic range don't qualitatively change the conclusion in this letter; see the forthcoming publication for more details [49].

**Summary**— In this letter, we predict the spin Hall effect (SHE) signature for the QCD matter created in relativistic heavy-ion collisions at RHIC-BES energies. Such SHE arises from the gradient of baryon chemical potential and is an essential mechanism generating spin polarization in baryon-rich QCD that has not been fully explored before. Using the freeze-out profiles from MUSIC hydrodynamics with AMPT initial conditions, we demonstrate that the SHE contribution to the differential Lambda polarization is comparable to those from the thermal vorticity and the shear-induced polarization (SIP) at lower collision energies. We propose to use the second harmonics of net spin polarization,  $P_{2,z}^{\text{net}}$  and  $P_{2,y}^{\text{net}}$  (defined in Eq. (4)), to detect the SHE. We predict that these proposed SHE observables will show the qualitative difference in both sign and collision energy dependence in the absence and presence of the SHE. Future experimental observation of the anticipated non-trivial signatures could provide the first evidence for the SHE in hot and dense QCD matter.

We gratefully acknowledge the contributions of Shuai Liu, who collaborated with us on this research project during its early stages. We thank helpful discussions with Francesco Becattini, Iurii Karpenko, Chun Shen and especially thank Xiangyu Wu for the code verification on the part of the results presented in this work. This work was supported in part by the NSFC under grant No. 12075007 (B.F. and H.S.), No. 12147173 (B.F.) and No. 11861131009, No. 12075098 (L.P.). Y.Y. thanks the support from the Strategic Priority Research Program of Chinese Academy of Sciences, Grant No. XDB34000000. We also acknowledge the extensive computing resources provided by the Supercomputing Center of Chinese Academy of Science (SCCAS), Tianhe-1A from the National Supercomputing Center in Tianjin,

China and the High-performance Computing Platform of Peking University.

---

\* fubaochi@pku.edu.cn

† lgpang@mail.ccnu.edu.cn

‡ huichaosong@pku.edu.cn

§ yiyin@impcas.ac.cn

- [1] M. Dyakonov and V. Perel, *Physics Letters A* **35**, 459 (1971).
- [2] J. Sinova, S. O. Valenzuela, J. Wunderlich, C. H. Back, and T. Jungwirth, “Spin hall effect,” (2014), arXiv:1411.3249 [cond-mat.mtrl-sci].
- [3] S. Murakami, N. Nagaosa, and S.-C. Zhang, *Science* **301**, 1348–1351 (2003).
- [4] Y. K. Kato, R. C. Myers, A. C. Gossard, and D. D. Awschalom, *Science* **306**, 1910 (2004).
- [5] J. Wunderlich, B. Kaestner, J. Sinova, and T. Jungwirth, *Phys. Rev. Lett.* **94**, 047204 (2005).
- [6] L. Liu, T. Moriyama, D. C. Ralph, and R. A. Buhrman, *Phys. Rev. Lett.* **106**, 036601 (2011).
- [7] M. König, S. Wiedmann, C. Brüne, A. Roth, H. Buhmann, L. W. Molenkamp, X.-L. Qi, and S.-C. Zhang, *Science* **318**, 766–770 (2007).
- [8] L. Adamczyk *et al.* (STAR), *Nature* **548**, 62 (2017), arXiv:1701.06657 [nucl-ex].
- [9] S. A. Voloshin, *EPJ Web Conf.* **171**, 07002 (2018), arXiv:1710.08934 [nucl-ex].
- [10] J. Adam *et al.* (STAR), *Phys. Rev. C* **98**, 014910 (2018), arXiv:1805.04400 [nucl-ex].
- [11] S. Acharya *et al.* (ALICE), *Phys. Rev. C* **101**, 044611 (2020), arXiv:1909.01281 [nucl-ex].
- [12] J. Adam *et al.* (STAR), *Phys. Rev. Lett.* **123**, 132301 (2019), arXiv:1905.11917 [nucl-ex].
- [13] S. Acharya *et al.* (ALICE), (2021), arXiv:2107.11183 [nucl-ex].
- [14] F. Becattini and M. A. Lisa, *Ann. Rev. Nucl. Part. Sci.* **70**, 395 (2020), arXiv:2003.03640 [nucl-ex].
- [15] F. Becattini and I. Karpenko, *Phys. Rev. Lett.* **120**, 012302 (2018), arXiv:1707.07984 [nucl-th].
- [16] I. Karpenko and F. Becattini, *Eur. Phys. J. C* **77**, 213 (2017), arXiv:1610.04717 [nucl-th].
- [17] Y. L. Xie, M. Bleicher, H. Stöcker, D. J. Wang, and L. P. Csernai, *Phys. Rev. C* **94**, 054907 (2016), arXiv:1610.08678 [nucl-th].
- [18] X.-L. Xia, H. Li, Z.-B. Tang, and Q. Wang, *Phys. Rev. C* **98**, 024905 (2018), arXiv:1803.00867 [nucl-th].
- [19] D.-X. Wei, W.-T. Deng, and X.-G. Huang, *Phys. Rev. C* **99**, 014905 (2019), arXiv:1810.00151 [nucl-th].
- [20] B. Fu, K. Xu, X.-G. Huang, and H. Song, *Phys. Rev. C* **103**, 024903 (2021), arXiv:2011.03740 [nucl-th].
- [21] Y. Guo, J. Liao, E. Wang, H. Xing, and H. Zhang, *Phys. Rev. C* **104**, L041902 (2021), arXiv:2105.13481 [nucl-th].
- [22] Y. Sun, Z. Zhang, C. M. Ko, and W. Zhao, (2021), arXiv:2112.14410 [nucl-th].
- [23] S. Y. F. Liu and Y. Yin, *JHEP* **07**, 188 (2021), arXiv:2103.09200 [hep-ph].
- [24] B. Fu, S. Y. F. Liu, L. Pang, H. Song, and Y. Yin, *Phys. Rev. Lett.* **127**, 142301 (2021), arXiv:2103.10403 [hep-ph].
- [25] F. Becattini, M. Buzzegoli, and A. Palermo, *Phys. Lett.*

- B **820**, 136519 (2021), arXiv:2103.10917 [nucl-th].
- [26] F. Becattini, M. Buzzegoli, A. Palermo, G. Inghirami, and I. Karpenko, (2021), arXiv:2103.14621 [nucl-th].
- [27] S. Y. F. Liu and Y. Yin, Phys. Rev. D **104**, 054043 (2021), arXiv:2006.12421 [nucl-th].
- [28] S. Ryu, V. Jovic, and C. Shen, (2021), arXiv:2106.08125 [nucl-th].
- [29] D. T. Son and N. Yamamoto, Phys. Rev. D **87**, 085016 (2013), arXiv:1210.8158 [hep-th].
- [30] Y. Hidaka, S. Pu, and D.-L. Yang, Phys. Rev. D **95**, 091901 (2017), arXiv:1612.04630 [hep-th].
- [31] Y. Hidaka, S. Pu, and D.-L. Yang, Phys. Rev. D **97**, 016004 (2018), arXiv:1710.00278 [hep-th].
- [32] K. Hattori, Y. Hidaka, and D.-L. Yang, Phys. Rev. D **100**, 096011 (2019), arXiv:1903.01653 [hep-ph].
- [33] C. Yi, S. Pu, and D.-L. Yang, (2021), arXiv:2106.00238 [hep-ph].
- [34] More precisely speaking, as shown in Ref. [27], the spin carriers' response to both electric field and  $\mu_B$  gradient are determined by the same retarded correlator between stress-energy tensor and axial Wigner function.
- [35] F. Becattini, V. Chandra, L. Del Zanna, and E. Grossi, Annals Phys. **338**, 32 (2013), arXiv:1303.3431 [nucl-th].
- [36] R.-h. Fang, L.-g. Pang, Q. Wang, and X.-n. Wang, Phys. Rev. C **94**, 024904 (2016), arXiv:1604.04036 [nucl-th].
- [37] Z.-W. Lin, C. M. Ko, B.-A. Li, B. Zhang, and S. Pal, Phys. Rev. C **72**, 064901 (2005), arXiv:nucl-th/0411110.
- [38] Y. He and Z.-W. Lin, Phys. Rev. C **96**, 014910 (2017), arXiv:1703.02673 [nucl-th].
- [39] L. Pang, Q. Wang, and X.-N. Wang, Phys. Rev. C **86**, 024911 (2012), arXiv:1205.5019 [nucl-th].
- [40] L.-G. Pang, H. Petersen, Q. Wang, and X.-N. Wang, Phys. Rev. Lett. **117**, 192301 (2016), arXiv:1605.04024 [hep-ph].
- [41] Z.-T. Liang and X.-N. Wang, Phys. Rev. Lett. **94**, 102301 (2005), [Erratum: Phys.Rev.Lett. 96, 039901 (2006)], arXiv:nucl-th/0410079.
- [42] J.-H. Gao, Z.-T. Liang, Q. Wang, and X.-N. Wang, (2020), arXiv:2009.04803 [nucl-th].
- [43] S. Y. F. Liu, Y. Sun, and C. M. Ko, Phys. Rev. Lett. **125**, 062301 (2020), arXiv:1910.06774 [nucl-th].
- [44] F. Videbaek (BRAHMS), Nucl. Phys. A **830**, 43C (2009), arXiv:0907.4742 [nucl-ex].
- [45] T. Anticic *et al.* (NA49), Phys. Rev. C **83**, 014901 (2011), arXiv:1009.1747 [nucl-ex].
- [46] W. Busza, K. Rajagopal, and W. van der Schee, Ann. Rev. Nucl. Part. Sci. **68**, 339 (2018), arXiv:1802.04801 [hep-ph].
- [47] J. Mohs, S. Ryu, and H. Elfner, J. Phys. G **47**, 065101 (2020), arXiv:1909.05586 [nucl-th].
- [48] When computing SHE quantitatively, we need to evaluate  $\nabla(\mu_B/T)$  on the freezeout surface which is related to  $n_B$  through  $T$  profile and EoS. Therefore, Fig. (1) (right) is presented only for illustrative purpose. Moreover, we notice that although  $\nabla n_B$  can be expressed in terms of a linear combination of  $\nabla T$  and  $\nabla\mu_B$ , the sign of  $\nabla n_B$  is not always the same as that of  $\nabla\mu_B$  because of non-trivial  $\nabla T$  profile, see Ref. [49] for details.
- [49] B. Fu, L. Pang, H. Song, and Y. Yin, "In preparation,".